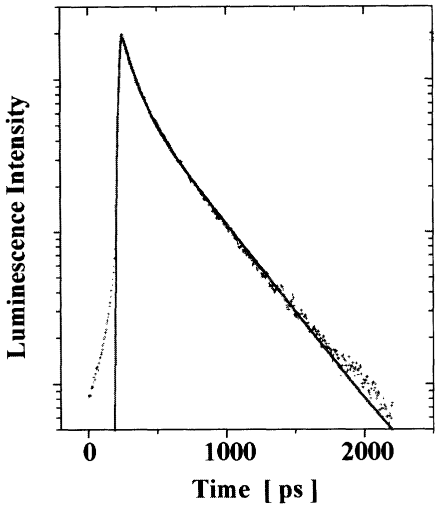

Fig. 4. The decay of the luminescence from the ZnO nanowires was studied with a frequency-tripled mode-locked Ti:sapphire laser for pulsed excitation (200-fs pulse length) and a streak camera with picosecond resolution for detection. A good fit (solid line) to the experimental data (dotted line) recorded at room temperature is obtained with a biexponential decay model assuming a fast and a slow process with time constants of ~70 and 350 ps, respectively. The time-resolved spectrum was recorded at an excitation power of 6.39 mW.

When the excitation intensity exceeds a threshold (~40 kW/cm^2), sharp peaks emerge in the emission spectra. The linewidths of these peaks are <0.3 nm, which are >50 times smaller than the linewidth of the spontaneous emission peak below the threshold. Above the threshold, the integrated emission intensity increases rapidly with the pump power (Fig. 3B). The narrow linewidth and the rapid increase of emission intensity indicate that stimulated emission takes place in these nanowires. The observed single or multiple sharp peaks represent different lasing modes at wavelengths between 370 and 400 nm. The lasing threshold is quite low in comparison with previously reported values for random lasing (~300 kW/cm^2) in disordered particles or thin films (*4*). These short-wavelength nanowire nanolasers operate at room temperature, and the areal density of these nanolasers readily reaches 1.1 × 10^{10} cm^{-2}.

The observation of lasing action in these nanowire arrays without any fabricated mirror prompts us to consider these single-crystalline, well-faceted nanowires as natural resonance cavities (Fig. 3C). It is possible that the giant oscillator strength effect (*8*), which can occur in high-quality nanowire crystals with dimensions larger than the exciton Bohr radius but smaller than the optical wavelength, enables the excitonic stimulated emission in these nanowire arrays. For II-VI semiconductors, the cleaved edge of the specimen is usually used as a mirror (*1–3, 17*). For our nanowires, one end is the epitaxial interface between the sapphire and ZnO, whereas the other end is the sharp (0001) plane of the ZnO nanocrystals. Both can serve as good laser cavity mirrors, considering that the refractive indexes for sapphire, ZnO, and air are 1.8, 2.45, and 1, respectively (*18*). This natural cavity or waveguide formation in nanowires suggests a simple chemical approach to forming a nanowire laser cavity without cleavage and etching. In fact, when multiple lasing modes were observed for these nanowires (Fig. 3A, inset), the observed mode spacing is ~5 nm for ~5-μm-long wires, which agrees quantitatively well with the calculated spacing between adjacent resonance frequencies $v_F = c/2nl$ (*17*), where v_F is emission mode spacing, c is the speed of light, n is the refractive index, and l is the resonance cavity length.

Furthermore, lifetime measurements (Fig. 4) show that the radiative recombination of the excitons is a superposition of a fast and a slow process with time constants of ~70 and 350 ps, respectively. The luminescence lifetime is mainly determined by the concentration of defects, which trap the electrons and/or holes and eventually cause their nonradiative recombination. Although the exact origin of the luminescence decay remains unclear at this stage, the long lifetime measured for these wires [350 ps, as compared with 200 ps for ZnO thin films (*4*)] demonstrates the high crystal quality achieved with the nanowire growth process.

References and Notes

1. D. A. Gaul, W. S. Rees Jr., *Adv. Mater.* **12**, 935 (2000).
2. M. A. Hasse, J. Qui, J. M. De Puydt, H. Cheng, *Appl. Phys. Lett.* **59**, 1272 (1991).
3. S. Nakamura *et al.*, *Jpn. J. Appl. Phys.* **35**, L74 (1996).
4. H. Cao *et al.*, *Phys. Rev. Lett.* **84**, 5584 (2000).
5. D. M. Bagnall *et al.*, *Appl. Phys. Lett.* **70**, 2230 (1997).
6. P. Yu *et al.*, *J. Cryst. Growth* **184/185**, 601 (1998).
7. C. Klingshirn, *J. Cryst. Growth* **117**, 753 (1992).
8. Y. Kayamura, *Phys. Rev. B* **38**, 9797 (1988).
9. W. Wegscheider *et al.*, *Phys. Rev. Lett.* **71**, 4071 (1993).
10. D. Mehus, D. Evans, *Laser Focus World* **31**, 117 (1995).
11. K. Haraguchi *et al.*, *Appl. Phys. Lett.* **60**, 745 (1992).
12. X. Duan, Y. Huang, Y. Cui, J. Wang, C. M. Lieber, *Nature* **409**, 66 (2001).
13. V. I. Klimov *et al.*, *Science* **290**, 314 (2000).
14. L. Pavesi, L. D. Negro, C. Mazzoleni, G. Franzo, F. Priolo, *Nature* **408**, 440 (2000).
15. M. H. Huang *et al.*, *Adv. Mater.* **13**, 113 (2001).
16. P. Fons *et al.*, *Appl. Phys. Lett.* **77**, 1801 (2000).
17. B. E. A. Saleh, M. C. Teich, Eds., *Fundamentals of Photonics* (Wiley, New York, 1991).
18. A simple estimation of the possible number of transversal modes that a waveguide can support indicates that our nanowires with diameters between 80 and 120 nm are actually single-mode waveguides for ultraviolet light.
19. This work was supported by the Camille and Henry Dreyfus Foundation, the 3M Corporation, the NSF through a Career Award (DMR-0092086), the U.S. Department of Energy, and the University of California, Berkeley. P.Y. is an Alfred P. Sloan Research Fellow. Work at the Lawrence Berkeley National Laboratory was supported by the Office of Science, Basic Energy Sciences, Division of Materials Science of the U.S. Department of Energy under contract DE-AC03-76SF00098. H.K. thanks the Swiss National Science Foundation for financial support. We thank the National Center for Electron Microscopy for the use of their facilities.

2 March 2001; accepted 26 April 2001

Ultraviolet Emission from a Diamond pn Junction

Satoshi Koizumi,[1]* Kenji Watanabe,[1] Masataka Hasegawa,[2] Hisao Kanda[1]

We report the realization of an ultraviolet light–emitting diode with the use of a diamond pn junction. The pn junction was formed from a boron-doped p-type diamond layer and phosphorus-doped n-type diamond layer grown epitaxially on the {111} surface of single crystalline diamond. The pn junction exhibited good diode characteristics, and at forward bias of about 20 volts strong ultraviolet light emission at 235 nanometers was observed and was attributed to free exciton recombination.

The wide energy band gap of diamond (5.47 eV) is attractive for the opto-electronic applications because it allows the possibility of ultraviolet (UV) light–emitting devices. Although diamond has an indirect band gap, cathodoluminescence (CL) and photoluminescence (PL) studies have revealed UV luminescence. The UV luminescence is related to exciton recombination from diamond crystals, which have high crystalline perfection. The main luminescence peaks appear at 5.27 eV (235 nm) for free exciton recombination with the assistance of transverse-optical (TO) phonon transition for intrinsic diamond (*1, 2*), and 5.21 eV (238 nm) (*1, 3*) and 5.18 eV (239 nm) (*4*) for bound exciton recombination for doped diamond. The energies of these luminescence peaks are considerably higher than those observed from gallium nitride (GaN) at 3.47 eV (357 nm). Recent studies provided

---

[1] Advanced Materials Laboratory, National Institute for Materials Science, 1-1 Namiki, Tsukuba 305-0044, Japan. [2] Research Center for Advanced Carbon Materials, National Institute of Advanced Industrial Science and Technology, Tsukuba Central 5, Tsukuba 305-8565, Japan

*To whom correspondence should be addressed. E-mail: KOIZUMI.satoshi@nims.go.jp

convincing evidence of free exciton recombination luminescence from high-quality diamond that can be observed even at room temperature by CL (*5*) and electroluminescence (*6*), whereas the other semiconducting materials exhibit the exciton related luminescence only at very low temperatures. This is considered to be due to large binding energy (80 meV) of free exciton in diamond. The result provides the possibility to realize UV light–emitting devices made of diamond. Concerning the impurity doping of diamond, doping with boron atoms (B doping) leads to p-type semiconducting diamond, which also exists in nature and can be reproducibly obtained by either chemical vapor deposition (CVD) or high-pressure growth techniques. Although n-type diamond does not exist in nature, thin films of n-type diamond have been grown by a CVD process with phosphorus (P) doping (*7*). We sucessfully grew both B- and P-doped diamond thin films on $\{111\}$ surfaces of diamond with high crystalline perfection. Here we report the formation of a pn junction diode along with the optical emission characteristics of the diode.

Each B- and P-doped diamond thin film was independently grown with the use of individual microwave plasma enhanced CVD systems. Metal chamber-type CVD systems with the background pressure of 1×10^{-8} torr were used to avoid incorporation of unexpected impurity such as silicon and nitrogen [see (*8*) for a detailed description]. Mechanically polished $\{111\}$ surface of B-doped single crystalline diamond with the resistivity of around 10^{-2} ohm·cm was used as a substrate. The size of the substrate is 2 mm^2 with 0.5-mm thickness. The steps of the formation process of pn structure are as follows: (i) cleaning of substrate surface, (ii) growing of B-doped layer, (iii) cleaning of the sample, (iv) growing of P-doped layer, (v) cleaning of the sample, and (vi) forming of ohmic electrodes for both the layers. For steps (i), (iii), and (v), a chemical oxidation process was applied using an acid mixture of $HClO_4$, H_2SO_4, and HNO_3 at a ratio of 1:3:4 and a temperature of 200°C for 30 min, resulting in the removal of nondiamond adsorbents from the sample surface and the termination of the surface with oxygen in place of hydrogen. Each B-doped and the P-doped layer was grown using trimethylboron [(TMB), $(CH_3)_3B$] and phosphine (PH_3), respectively, as impurity source gases (*9*, *10*). The electrical properties of each layer have been characterized by Hall measurements using the layers grown simultaneously on separate insulating diamond substrates, with p-type and n-type conductivity confirmed for B-doped and P-doped layers and showing a carrier activation energy of 0.37 and 0.59 eV, respectively. These values are in good agreement with the published data for those impurity-doped diamonds (*8*, *11*). The carrier mobility of the B-doped and the P-doped layer is 300 cm^2/V·sec and 60 cm^2/V·sec, respectively, at room temperature. Lastly, the ohmic electrodes were formed for both the p-type and n-type layers. For the p-type layer, we deposited a Ti film (thickness 100 nm) with a Au evaporated film (also 100 nm thick) for protection. The films were deposited at 400°C to make a better ohmic interface. For the n-type layer, Ar ion implantation was performed (*12*, *13*) through a mask to make graphitic dots with a depth of 30 nm and a diameter of 150 μm at 20 to 25 different points on the surface. The acceleration voltage and the dose were 40 keV and 10^{16} cm^{-2}, respectively. The implanted dots were covered by Ti and capped with Au film for protection. The sample was annealed in high vacuum (5×10^{-6} torr) at 850°C for 1 hour to ensure the stability of the implanted contacts during diode operation. The annealing process does not affect the electrical properties of the p-type and n-type layers. Also, at such annealing temperature we do not expect appreciable inter-diffusion of impurities through the pn junction. To check the impurity concentrations of each layer and interdiffusion, secondary ion mass spectrometry (SIMS) analysis was performed for the pn structure grown on insulating diamond substrate at the same growth condition (Fig. 1). The impurity concentrations of B-doped and P-doped layers are 1 to 2×10^{17} cm^{-3} and 7 to 8×10^{18} cm^{-3} and thicknesses of about 1 and 2 μm, respectively. The doping profile is almost uniform for each P- and B-doped layer, and there is no intermixture region at the pn interface.

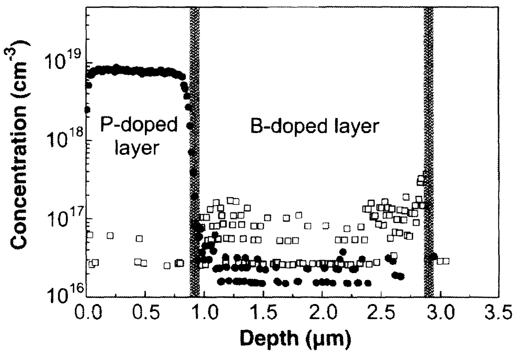

Fig. 1. Impurity depth profile of pn junction measured by SIMS, where solid circles represent phosphorus (^{31}P) and open squares represent boron (^{11}B).

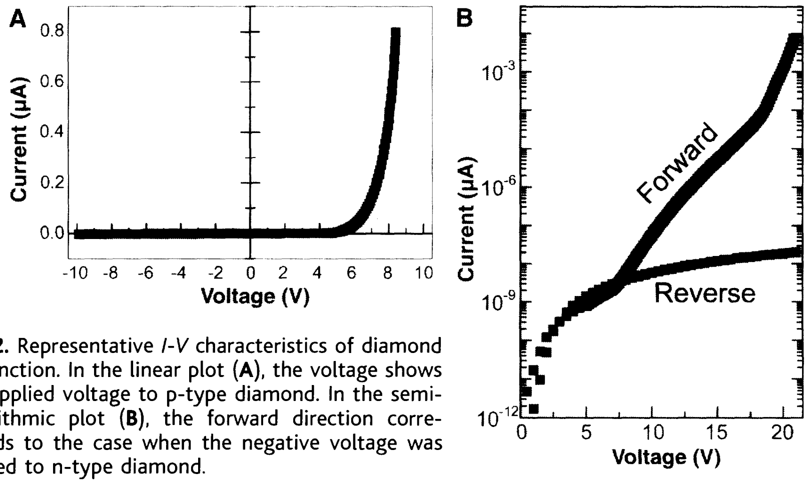

Fig. 2. Representative *I-V* characteristics of diamond pn junction. In the linear plot (**A**), the voltage shows the applied voltage to p-type diamond. In the semilogarithmic plot (**B**), the forward direction corresponds to the case when the negative voltage was applied to n-type diamond.

Current-voltage (*I-V*) characteristics of the pn junction show clear rectifying property (Fig. 2A). The rectification ratio was about three orders of magnitude when forward (n-type negative) and reverse (n-type positive) voltage applied at ±15 V (Fig. 2B). The reverse current is rather high (about 10^{-8} A at −20 V) due to the imperfection of the junction at specific portions of the sample. Due to the large reverse current, the turn-on voltage (6 to 7 V) is observed at a higher than expected value (4 to 5 V). A strong deviation of the *I-V* profile from the exponential relation over an applied voltage of 10 V is due to high series resistance of the sample (mainly of the P-doped layer) of more than 10^6 ohms. When the forward current exceeds 10^{-4} A, the temperature of the sample rises by spontaneous resistive heating, and, as a result, the *I-V* profile becomes steeper. The capacitance-voltage characteristic shows an increase of capacitance according to the

Fig. 3. Optical emission spectra of the pn junction operated with forward current of (**A**) 1, (**B**) 5, and (**C**) 10 mA. A representative CL spectrum of P-doped diamond thin film taken at room temperature is shown in (**D**). The inset is a representative optical image of the diamond LED with light emission. The circular-shaped electrodes (diameter, 150 μm) are formed by the separating each other by 150 μm. Light emission can be seen around the electrode located at the center of the image.

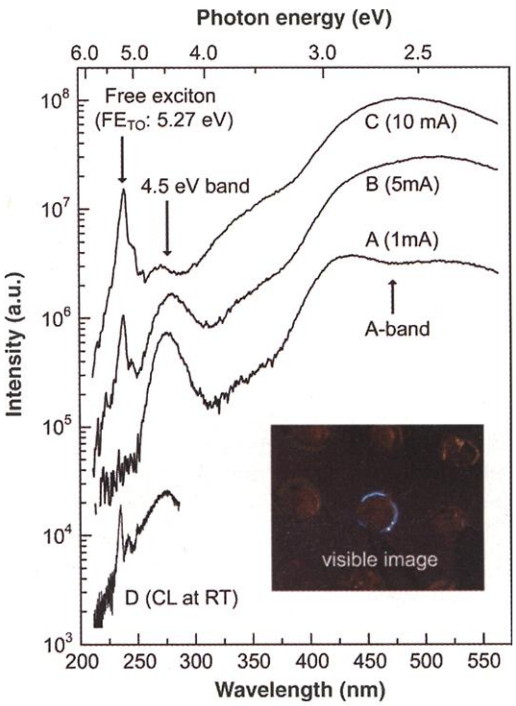

increase of the voltage in a reverse voltage region, confirming the existence of a depletion layer and its narrowing according to the voltage increase.

For forward currents exceeding 0.1 mA, light emission was observed. In the present structure of the samples, light emission was observed around the electrode of the sample because the pn junction and the light-emitting area exist behind the electrode and because the driving voltage is applied perpendicular to the sample surface (Fig. 3 inset). As we increased the forward current, we observed the UV light emission in the spectrum (Fig. 3). The driving voltages were 20 V for 1 mA, 21.5 V for 5 mA, and 23 V for 10 mA. For the present sample, over 5 mA, we saw a sharp emission peak located at 235 nm (5.27 eV), which is attributed to free exciton recombination luminescence coupled with TO phonon ($\mathrm{FE_{TO}}$) (Fig. 3, B and C). The small peak (shoulder) located at around 243 nm (5.10 eV) is attributed to the phonon replica of $\mathrm{FE_{TO}}$ peak. Also observed were broadband emissions at an UV region with peak energy located at 4.5 eV and a broadband emission in the visible region. The origin of a 4.5-eV band emission is not very clear yet, but it is often observed for B- and P-doped CVD diamond thin films by CL and PL analysis (*3*, *4*). The band emission in the visible region is attributed to A-band emission that is often observed by CL and PL from CVD diamond thin films. The intensity ratio of the free exciton peak against the A band was 1:7 for a forward current of 10 mA (Fig. 3C). The appearances of the free exciton and the 4.5-eV band emissions are very consistent with room temperature CL spectrum observed from P-doped diamond thin film (Fig. 3D). This result supports high crystalline perfection of the P-doped layer prepared here. In our series of B-doping experiments for {111} diamond thin films, the quality of the B-doped layer was not so good, such that the exciton peak bound to boron was negligibly weak, even at 110 K. The visible lights such as A-band luminescence observed in the spectrum are most likely emitted from B-doped layer. By further improving the crystalline quality of the B-doped layer, the A-band emission will be suppressed and a diamond light-emitting diode (LED) that exclusively emits monochromatic UV light of 235 nm will be feasible.

References and Notes

1. P. J. Dean, E. C. Lightowlers, D. R. Wight, *Phys. Rev.* **140**, A352 (1965).
2. A. T. Collins, M. Kamo, Y. Sato, *J. Phys. Condens. Matter* **1**, 4029 (1989).
3. S. C. Lawson, H. Kanda, H. Kiyota, T. Tsutsumi, H. Kawarada, *J. Appl. Phys.* **77**, 1729 (1995).
4. H. Sternschulte, K. Thonke, R. Sauer, S. Koizumi, *Phys. Rev. B* **59**, 12924 (1999).
5. H. Watanabe *et al*, *Appl. Phys. Lett.* **73**, 981 (1998).
6. H. Horiuchi, K. Nakamura, S. Yamashita, *Jpn. J. Appl. Phys.* **39**, L604 (2000).
7. S. Koizumi, H. Ozaki, M. Kamo, Y. Sato, T. Inuzuka, *Appl. Phys. Lett.* **71**, 1065 (1997).
8. S. Koizumi, T. Teraji, H. Kanda, *Diamond Relat. Mater.* **9**, 935 (2000).
9. H. Maeda *et al.*, *Diamond Relat. Mater.* **7**, 88 (1998).
10. M. Kamo, H. Yurimoto, T. Ando, Y. Sato, *Proceeding of the Second International Conference on New Diamond Science and Technology* (Materials Research Society, Pittsburgh, PA, 1991), pp. 637–641.
11. S. Yamanaka *et al.*, *Jpn. J. Appl. Phys.* **37**, L1129 (1998).
12. J. Prins, *J. Phys. D* **22**, 1562 (1989).
13. T. Teraji, S. Koizumi, H. Kanda, *Appl. Phys. Lett.* **76**, 1303 (2000).
14. The authors express their gratitude to S. Yamanaka and H. Okushi for the technical assistance of the electrical measurements; to K. Tanabe, K. Nakazawa, and H. Kawarada for cathodoluminescence analysis; and to J. Chevallier for SIMS analysis.

27 February 2001; accepted 2 May 2001

(Amino)(Aryl)Carbenes: Stable Singlet Carbenes Featuring a Spectator Substituent

**Stéphane Solé,[1] Heinz Gornitzka,[1] Wolfgang W. Schoeller,[2]
Didier Bourissou,[1] Guy Bertrand[1]***

Several (amino)(aryl)carbenes have been shown to be stable at room temperature in solution and in the solid state. Electroneutrality of the carbene center is ensured by the amino group, which has both π-donor and σ-acceptor electronic character. The aryl group remains a spectator substituent, as shown by single-crystal x-ray analysis and by its chemical behavior. Because only one electron-active substituent is needed, numerous stable carbenes will become accessible, which will open the way for new synthetic developments and applications in various fields.

Attempts to prepare the parent carbene (CH_2) by dehydration of methanol were reported as early as the 1830s (*1*). At that time, the tetravalency of carbon had not been established, and therefore the existence of stable carbenes was considered to be quite reasonable. Carbenes were only recognized as reactive intermediates some 50 years later (*2*, *3*), at which time it quickly became clear that their six-valence-electron shell, which defied the octet rule, was responsible for their fugacity. Thus, the quest for stable carbenes became an unreasonable target and remained so for quite some time, although these transient species found numerous applications in synthetic chemistry (*4*–*7*).

In the last 15 years, the preparation of persistent triplet carbenes **I** (*8*) and the isolation at room temperature of singlet carbenes **II** and **III** (Fig. 1) represent spectacular